ISSUE: January 2013

Hardware-In-The-Loop System Eases Development And Testing Of Grid-Connected Power Electronics Applications

by Evgenije Adzic, Vlado Porobic and Nikola Celanovic, Typhoon HIL, Novi Sad, Serbia

The introduction of renewable energy sources such as photovoltaic (PV) power at the utility level poses significant challenges in the design and development of the associated power electronics. The power electronics technologies and control concepts required to properly integrate these technologies into the utility power system are continually being developed to fully realize their benefits, while avoiding the potentially negative impacts these technologies could have on system safety and reliability.

The existing approaches to developing power electronics for grid connection often fall short in terms of design verification, productivity, and cost. Ultimately, these issues do affect the adoption of renewable energy in the marketplace. To support the production and delivery of clean electricity, there is a critical need to have a single development and test environment that would allow verification of standard technical requirements set for grid-connected power electronics systems.

Typhoon HIL addresses that critical need by providing a uniform environment for evaluation of requirements relevant to the performance, operation, and testing of the grid-connected converter's control system. The key component in such an environment is a hardware-in-the-loop (HIL) emulator, which executes in real-time a mathematical model representing the real power electronics converter and the grid system, while the real-time control code is executed on real controller hardware that interfaces directly with the HIL emulator.

In this article, we use the Typhoon HIL 400 high-fidelity emulator (Fig. 1), which provides enough computational power to execute models of the switching power converter stage and power grid in 1-µs time steps. The emulator communicates via an Ethernet or USB data link to a system computer with a sophisticated Typhoon HIL software tool-chain that provides an intuitive, flexible and easy-to-use interface for controlling the test process.

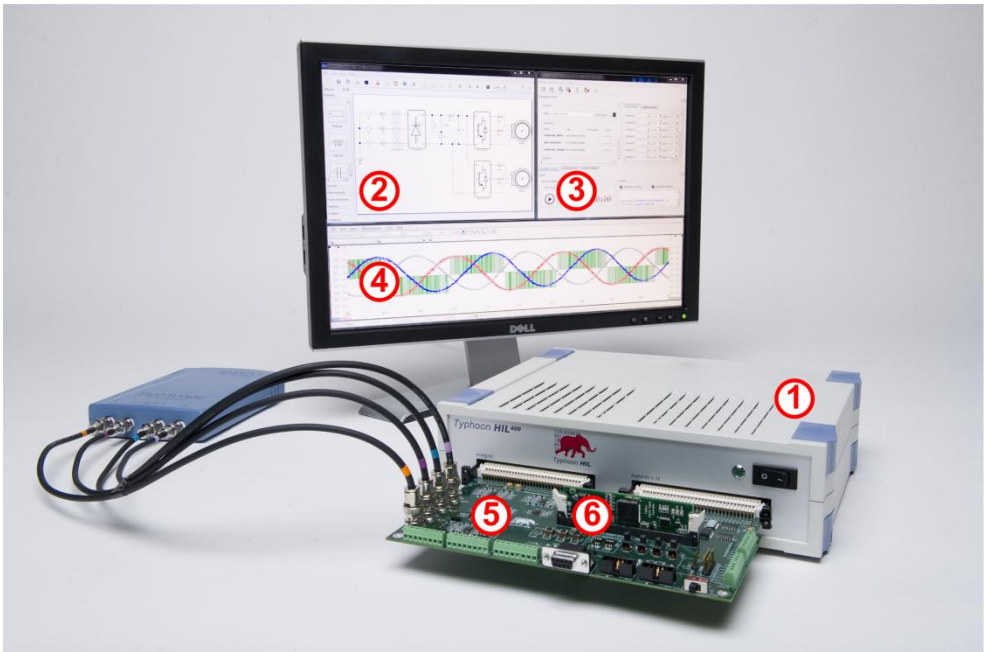

Fig. 1. The Typhoon HIL development and testing environment includes the HIL emulator (1), the Schematic Editor/Circuit Compiler (2), the HIL Control Panel (3), the Capture Signal Panel (4, only offered in the HIL600 system, an external oscilloscope here), the Interface board (5, here, the TI Docking Station), and the controller under test (6, here the TMS320F2808 Control Card).

With this approach, the topology of an emulated power electronics circuit as well as the parameters of the circuit can be easily modified in Typhoon's Schematic Editor/Compiler, using a comprehensive library of elements and corresponding block dialogues. An HIL Control Panel represents another intuitive graphical user interface (GUI) software component that allows the user to set up the HIL emulation parameters, run and stop the emulation, select model signals for controller feedback and variables to be observed on a signal oscilloscope, set up HIL output signals scaling/offset and change model parameters online.

A controller under test can be connected directly to the digital and analog I/O connectors of the HIL emulator via a custom-made interface board or a flexible Typhoon HIL Universal Interface Board to accommodate a variety of industrial controllers. In this article we use the Typhoon HIL TI Docking Station, which represents a plug-in interface board between the HIL emulator and any of Texas Instruments' DIMM100-compatible control cards like the TMS320F2808 used in the example presented here.

The power electronics circuit and corresponding control strategy, which will be evaluated in this article, are given in Fig. 2. This particular example is based on a project in which the HIL environment was used to develop control software for a PV single- and three- phase grid-inverter application. But note that the Typhoon HIL platform is not restricted only to research and development and quality assurance qualification of grid-connected converter control systems. This platform is flexible enough to accommodate a variety of power electronics systems such as electrical machine drives and switching power supplies.

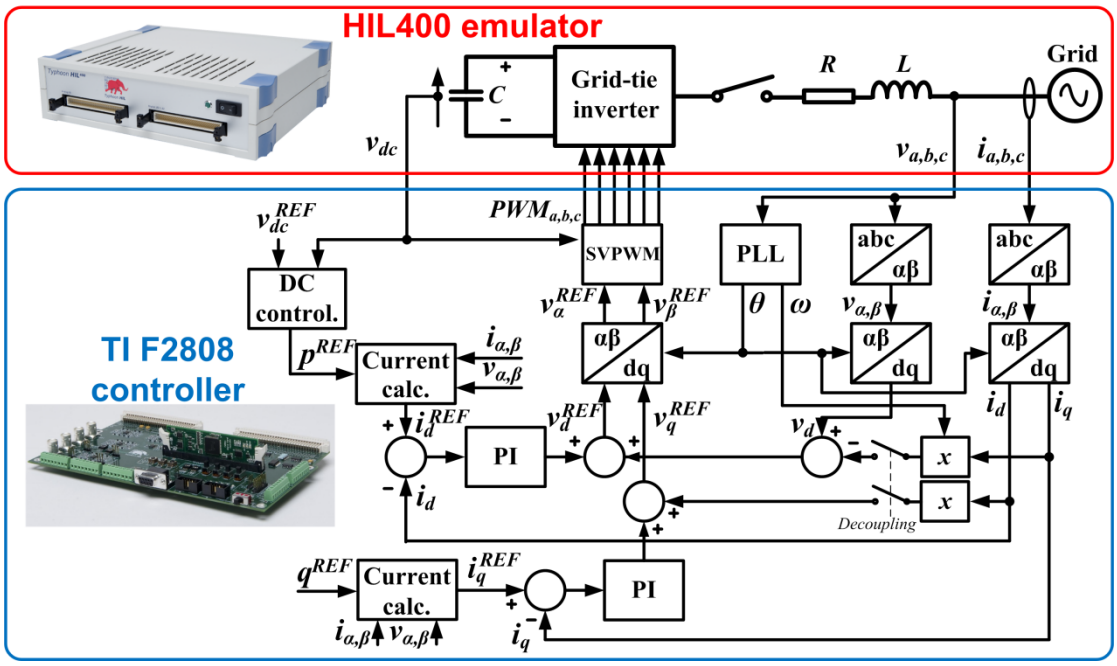

Fig. 2. Control scheme implemented on the TI F2808 control card used in Typhoon HIL Grid-Connected Converter demo application.

Grid-Connected Converter-Control Structure

Technical background

The main task of a grid-connected converter is to provide controlled injection of both active and reactive power into the grid, independently. In order to achieve proper power-flow regulation, the vector control principle with grid voltage vector orientation is widely used. The control strategy incorporated in a large number of distributed-generation converter units is shown in Fig. 2 (blue frame).

This control strategy is based on reference frame theory, where grid currents and voltages are transformed into a reference frame rotating synchronously with the grid voltage. A phase-locked loop (PLL) provides the phase angle of the grid voltages required for the synchronization. As a consequence, the control variables (grid currents and voltages) appear as dc values, also called dq-components.

In such a system, grid current dq-components independently determine active and reactive power flow to the grid. The dq-current control structure is usually associated with proportional-integral (PI) controllers in order to obtain simplicity and robustness in regulating the dc variables. In terms of achieving converter protection and the desired active and reactive power flow between the power converter and the grid, a current loop is responsible for power quality issues.

The control structure also incorporates an outer dc link voltage control loop in the active power flow control path, which maintains the dc link voltage at a desired reference value. An active power transfer reference command (p^{REF}) comes from the output of the dc link voltage controller and a reference reactive power (q^{REF}) is usually set to 0. Following this, the task of the dc voltage controller is to transfer all incoming dc link energy to the grid and to achieve unity power factor. In that way, inverter-based distributed power generators, like photovoltaic (PV) inverters, achieve active power transfer to the grid.

Real-Time Implementation

The power electronics system hardware under consideration is emulated in real time on the HIL400 platform with a time-step of 1 μs. The model of the PWM inverter, dc link and electrical grid are simulated using the HIL400 (Fig. 2, red frame), while the control algorithm with a PWM carrier frequency of 4 kHz is implemented using a control platform based on the Texas Instruments TMS320F2808 digital signal processor (Fig. 2, blue frame).

Using the intuitive Schematic Editor and its comprehensive library of parameterized elements, it is easy to directly specify the desired power electronics system hardware (Fig. 3). With one click of a button, a model is compiled, downloaded to the HIL emulator and ready for control.

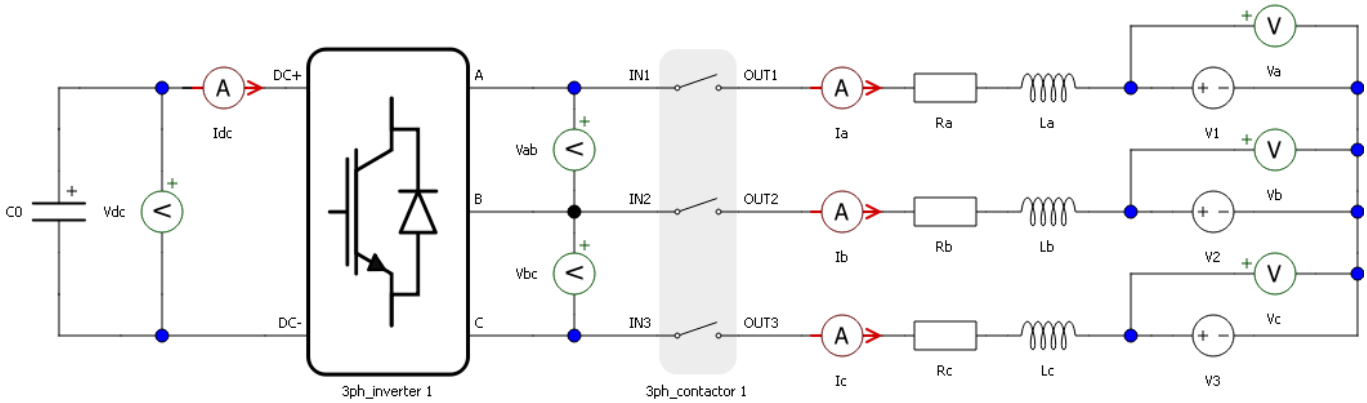

Fig. 3. A three-phase grid connected power converter circuit in the Schematic Editor.

Through inverter and contactor schematic blocks, the user can assign HIL digital inputs for fetching the gate drive and control signals from the controller. On the other hand, measurement elements like ammeters and voltmeters, can be placed anywhere in the circuit model to provide controller feedback signals at HIL analog outputs or just monitoring signals from the oscilloscope. Here, the controller measures the dc link voltage (Vdc), grid phase voltages (Va, Vb, and Vc) and grid phase currents (Ia, Ib, and Ic) to implement the given cascaded grid voltage vector-oriented control structure.

The grid is modeled as voltage sources V1, V2 and V3 (grid phases a, b and c, respectively). The HIL Control Panel allows the user to configure simulated grid sources in the model, by specifying arbitrary magnitude, frequency and phase shift values for ideal sinusoidal grid voltages. Additionally, the user can completely and freely program the grid voltage waveform by defining each voltage level in a time-window of the waveform period or can use the Waveform Editor to produce standard utility power disturbances such as voltage sags, spikes, phase angle jumps, magnitude ramp, frequency change or harmonic distortion. In that way, the user can easily conduct standard controller tests in grid-connected power electronics applications (such as such specified by the National Electric Code and IEEE 1547) by initiating grid disturbances through the HIL Control Panel.

Note that, for these types of tests, the Typhoon HIL environment is distinguished from the traditional approach where expensive hardware test equipment like ac power sources for grid simulation are used. This system

enables the user to build a completely safe test installation for a megawatt (MW) level grid-connected inverter at your office desk, without the need for paralleling expensive hardware test equipment. This capability simultaneously eliminates all safety and cost issues with regard to the laboratory test set. In parallel, it allows the user to focus on the evaluation of the software-based functionalities, which are provided by the inverter's controller, in order to satisfy most of the technical specifications established for grid-connected converter systems.

Synchronization Unit Test

Technical background

In the presented vector control algorithm, it is necessary to accurately and precisely determine the grid voltage phase angle (θ) in order to achieve independent control of active and reactive power transfer between the converter dc link and the grid. This task is performed by a grid synchronization unit.

The quality of the grid synchronization, in addition to current regulators in the control structure, is a key factor that determines the overall quality of the control structure. Error in the phase angle estimation can lead to significant errors in the imposed converter output voltage, and thus the error between the reference and injected power (current) into the grid.

In the literature on grid synchronization, one finds that different methods are applied in practice for grid-connected converters. The most common method used today is the phase-locked loop (PLL) implemented in the dq-synchronous rotating reference frame, shown in Fig. 4a.

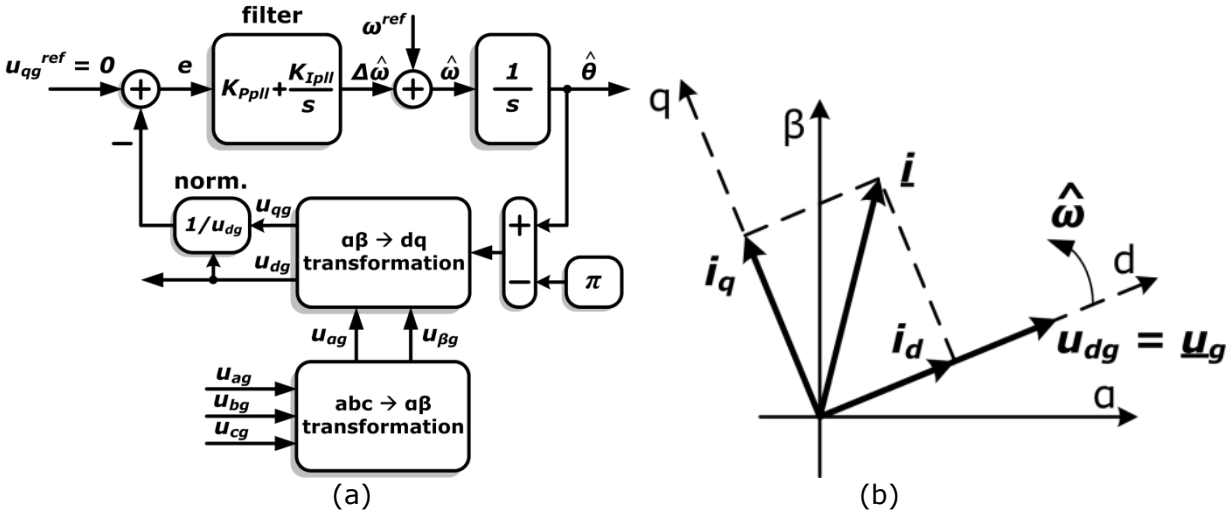

Fig. 4. Conventional dq-PLL system block diagram (a) and vector diagram of grid-connected converter variables in dq-reference frame (b).

This PLL system contains a filter, usually proportional-integral (PI) controller type, that determines the PLL's dynamic behavior. An error signal (*e*) is formed by subtracting the actual grid voltage q-component (u_{qg}) (which is obtained using estimated angle ($\theta\hat{}$)) from the reference grid voltage q-component (u_{qg}^{ref}) (which is set to 0). The PI controller will act to reduce the error (*e*) to zero, which would lead to equalization of the estimated phase angle and actual grid-voltage phase angle, in steady state. In that case, the grid voltage d-component (u_{dg}) is equal to the grid voltage amplitude (u_g), and the rotating reference frame is aligned with the grid voltage vector (Fig. 4b.) The normalization block ($1/u_{dg}$) is usually introduced in order to avoid gain loss and possible instability during grid voltage sags.

The PLL is especially influenced by the presence of unbalance, harmonic distortion and measurement offsets in the grid voltages. Therefore, the filter bandwidth has to be carefully chosen as a compromise between two goals. On the one hand, the PLL needs to filter undesirable harmonics that occur in the PLL control system due to voltage distortion. Other the other hand, the PLL should have the fast response time necessary for tracking

voltage during frequency changes or voltage sags in the grid. It can be shown that for critical-aperiodic PLL response, the filter parameters (K_{Ppll} and K_{Ipll}) have to be set to these values:

$$K_{p_{pll}} = \sqrt{2}\omega_{bw}$$

$$K_{I_{pll}} = \frac{\omega_{bw}^2}{2}$$

where ω_{bw} is desired PLL system bandwidth. For a desired frequency bandwidth of 3 Hz, the expected settling time of PLL angle response would be around 1 s. This can be evaluated using the Typhoon HIL environment, which can also be used to verify other aspects of the intended PLL behavior during various grid disturbances.

Experimental Results

Among the external control options for the controller under test, the HIL Control Panel allows the user to manually control switches in the emulated model by means of software. In this test phase, it is helpful to control the grid contactor manually via software (Fig. 5a). In this test phase, we want to examine only how the PLL determines phase angle from measured grid voltages, and not how the converter injects currents into the grid.

In the Source settings section of the HIL Control Panel, the user can configure all sources in the model. In this case, the sources are grid voltage waveforms V1, V2, and V3. At first, we selected the Sine waveform option for generating pure sinusoidal voltages with 230-V rms magnitude and 50-Hz frequency (Fig. 5b), to examine PLL operation under ideal grid-voltage conditions. One can note that phase-shift values are set to produce a balanced three-phase set of grid voltages (0°, -120°, and -240°.)

After starting emulation, the user can observe selected model variables on the scope in real-time. Fig. 5b shows grid voltages in the model, where HIL analog output scaling for those variables was set in the Analog outputs section of the HIL Control Panel to 100 V/V_{HIL}. In practice, using the oscilloscope one can read signal amplitudes of 3.25 divs, which—for selected scope scaling (1 V/div) and HIL analog output scaling (100 V/V_{HIL}) —yields a real voltage amplitude of 325 V (in accordance with the set magnitude of 230 Vrms.)

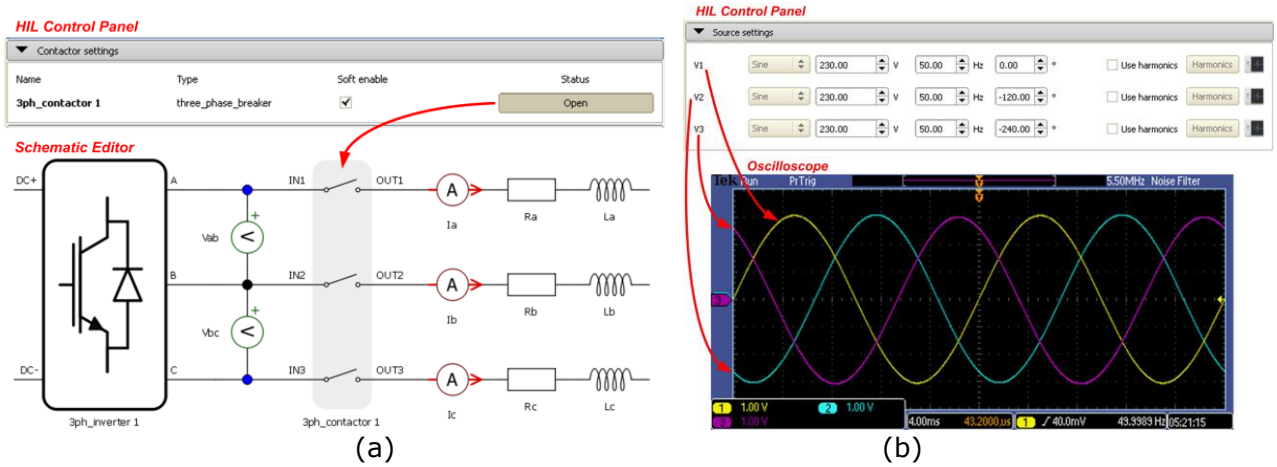

Fig. 5. All model switches in the model can be manually controlled through the HIL Control Panel (a). All model sources can be easily configured to generate desired waveforms (b).

In order to test PLL dynamic behavior, the Waveform Generator was used to produce a standard disturbance in the form of a grid-voltage phase jump. An input value of 180° was set as the desired phase jump and one of the HIL digital outputs was used to trigger the oscilloscope to capture the defined grid voltage transient, shown in Fig. 6a.

The same HIL digital output was used to trigger data capture on the controller. Through a specialized Typhoon TI Control Panel software component, which presents an interactive interface for controlling the Texas Instruments C2000 DSPs through a serial link, data can be collected and plotted using the integrated Matplot library. Recorded results showing relevant variables in the controller for PLL evaluation are given in Fig 6b.

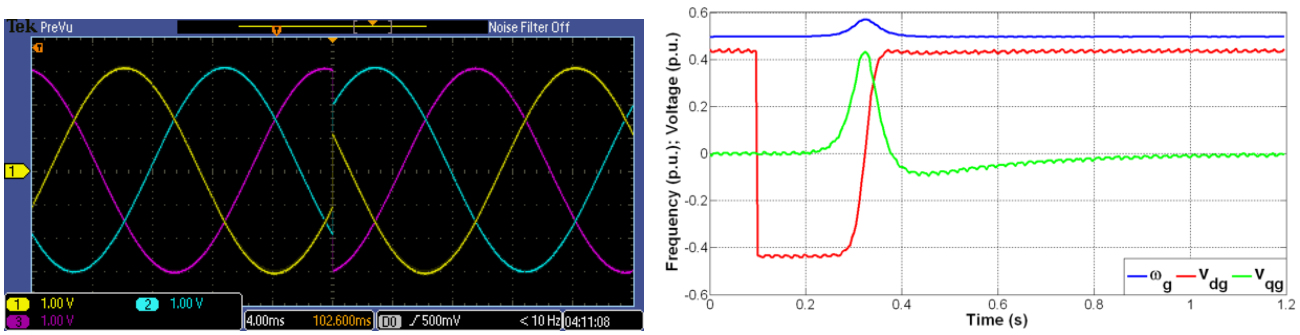

(a) (b)

Fig. 6. A grid-voltage phase jump is generated in the model to test PLL transient response (a) and the relevant controller variables for PLL transient evaluation are recorded (b).

Fig. 6b shows that the grid voltage q-component (v_{qg}) is equal to 0, and that the d-component (v_{dg}) is equal to the grid-voltage amplitude 0.433 p.u., before the grid-voltage phase jump and after the transient response (controller voltage base value is 750 V.) That indicates proper PLL operation in steady-state. It can be concluded that the grid-voltage components are dc values, which is a consequence of the chosen control strategy.

Transient response is in accordance with design requirements: without overshoot, which can be observed in voltage d-component, and with a settling time around 0.8 s, which can be observed in voltage q-component. The estimated frequency (ω_g) is exactly 0.5 p.u. in steady-state, which gives 50 Hz knowing that a frequency base value of 100 Hz is used in the controller.

The next step is to verify the PLL algorithm under highly distorted grid-voltage conditions. Fig. 7 shows the grid voltage waveforms used in the emulation.

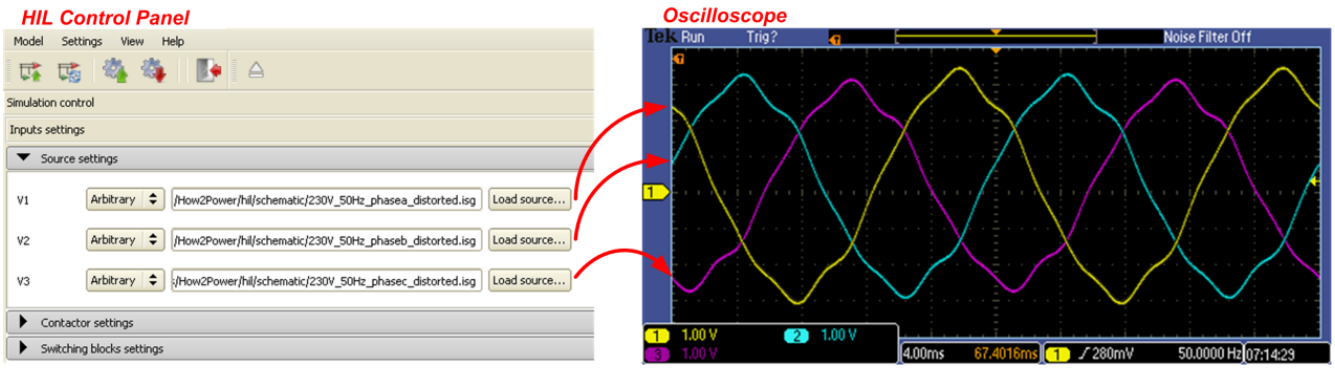

(a) (b)

Fig. 7. Grid voltage sources are configured to an arbitrary waveform (a). Distorted grid voltages are generated in the model used for PLL evaluation under distorted grid voltage conditions (b).

In the Source settings section of the HIL Control Panel, the Arbitrary waveform option was selected and file (.isg) which contains waveform information on unbalanced and distorted grid voltage with introduced offset was specified. The arbitrary waveform (.isg file) can be generated easily using the Waveform Generator tool. The grid is distorted with 5th and 7th harmonics, each with an amplitude equal to 3.5% of the fundamental. In that way, the total harmonic distortion (THD) of the simulated grid voltage is 5%, which represents the maximum allowed value of voltage THD in the distribution grid.

The phase shift of the harmonics is set in order to have a typical waveform of the distribution grid voltage at which the power converter is connected. Unbalance above 5% is additionally introduced in the grid voltage waveforms, by setting the phase-b fundamental amplitude to 95% and the phase-c amplitude to 90% compared to the amplitude of the phase-a voltage. The possible signal offset introduced by the measurement and conversion circuits in real converters was also simulated by introducing an additional offset of 5% in the generated waveforms.

The results recorded from the controller, which are presented in Fig. 8, show the PLL steady-state response under the given distorted grid-voltage conditions. The response is shown for two different sets of PLL filter parameters. Fig. 8a shows the estimated grid-voltage angle (θ_g), estimated grid-voltage frequency (ω_g), and measured grid phase-a voltage (v_{ag}) for the PLL bandwidth setting of 3 Hz. Fig. 8b shows the same variables for the case where bandwidth is set to 50 Hz.

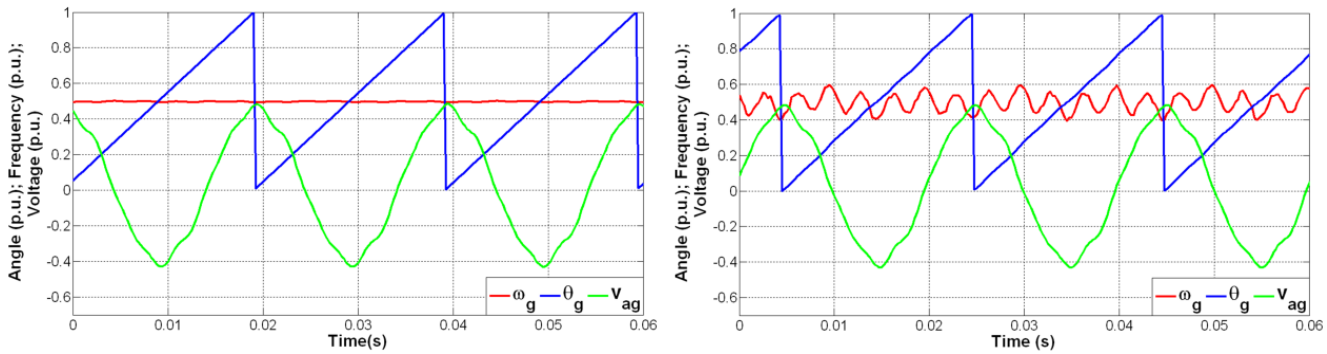

(a) (b)

Fig. 8. PLL steady-state response under distorted grid-voltage conditions for a designed bandwidth of 3 Hz (a) and for a designed bandwidth of 50 Hz (b).

Note the importance of properly selecting PLL filter parameters in order to attenuate the possible propagation of harmonics (caused by grid-voltage distortion) through the PLL system. In the case of the designed PLL bandwidth of 50 Hz, it cannot adequately reject the influence of grid-voltage distortion as reflected in the estimated frequency waveform seen in Fig. 8b. One can observe 50-Hz, 100-Hz and 300-Hz harmonic components in the estimated frequency variable (ωg), producing an estimated angle signal (θ_g) that significantly deviates from a pure ramp waveform.

Current Control Loop Test

Technical background

In order to implement current control, a mathematical model of a grid-connected converter will be introduced here. The electrical circuit of the system is shown in Fig. 9.

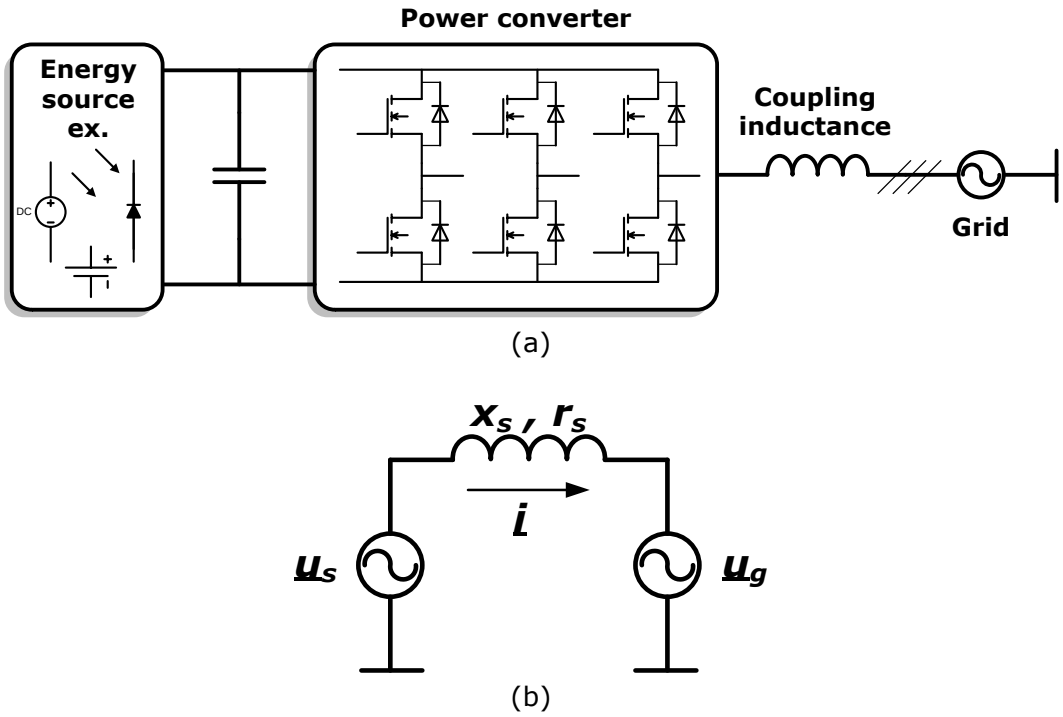

Fig. 9. A grid-connected converter (a) and its simplified electrical representation (b).

Equations in original phase domain can be easily transformed in the stationary reference frame ($\alpha\beta$) and synchronously rotating (dq) frame, rotating at the PLL estimated frequency (ω_G). Absolute variables can be transferred in a normalized (relative) domain using selected and derived base values (e.g. V_B – base voltage, I_B – base current, ω_B – base angular frequency, etc.).

The PLL place grid-voltage space vector in the d-axis of the rotating-frame, and the state-space model of the system can be described by equations (1)-(7). The active and reactive power (amplitude invariant dq system), along with the dc-link voltage are given by equations (4)-(6).

[N – normalized (relative) values]:

$$\tau_S \frac{di_d}{dt} = -r_S i_d + \omega_G l_S i_q + u_{dS} - u_{dG} \quad (1)$$

$$\tau_S \frac{di_q}{dt} = -r_S i_q - \omega_G l_S i_d + u_{qS} \quad (2)$$

$$\frac{1}{f_B}\frac{d\theta_G}{dt} = \omega_G \quad (3)$$

$$p_G = \frac{3}{2} u_{dG} i_d \quad (4)$$

$$q_G = \frac{3}{2} u_{dG} i_q \tag{5}$$

$$u_{DC} = \frac{\omega_B}{C} \int i_C dt \tag{6}$$

where variable τ_S is a grid-equivalent time-constant:

$$\tau_S = \frac{L_S}{Z_B} \tag{7}$$

and all the rest of the variables are normalized representatives of their absolute values $\left(x_N = \frac{x_A}{x_B} \right)$.

According to the voltage equations (1) and (2), cross-coupling terms are present between *dq*-axes (current in direct *d*-axis has effects on the current in the quadrature *q*-axis and vice versa). Therefore, the decoupling scheme given by equations (8) and (9) has to be applied in the current-control structure. Embedding the cross-coupling and voltage feed-forward terms in the PI controller structure as depicted in the Fig. 10, is usually reported as improving the harmonic compensation capability of the control structure being considered.

Transformation angle θ_G^{est} is obtained from the grid synchronization unit and it was discussed before in detail.

$$u_{ds} = u_{ds}^{ref} - \omega_G l_S i_q + u_{dG} = u_{ds}^{ref} + u_{ds}^{decouple} \tag{8}$$

$$u_{qs} = u_{qs}^{ref} + \omega_G l_S i_d = u_{qs}^{ref} + u_{qs}^{decouple} \tag{9}$$

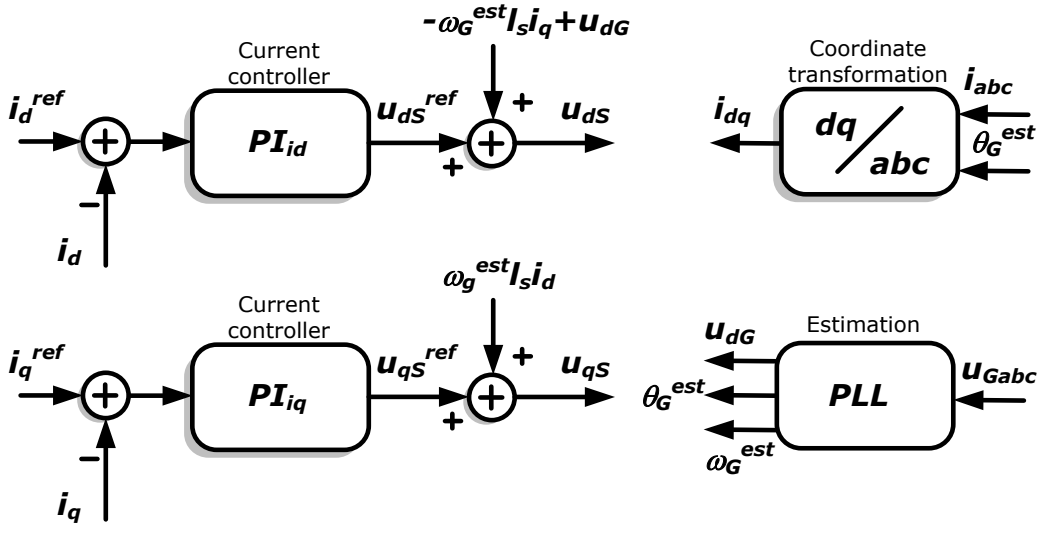

Fig. 10. Current-control strategy for grid-connected-converter.

Fig. 11 shows the control loop for current *d*-component after application of decoupling elements. Also, the quadrature *q*-axis current loop has the same layout ($\tau_S = \tau_S / r_S$ —grid time constant, τ_i —sampling period.)

Thus, PI controller parameter values for both axes are identical. They can be determined by any of the proposed methods in the relevant literature, such as application of Dahlin's algorithm as used in this example. This approach assumes that the controlled object has first-order delay and transportation delay, which is exactly the case with the current-control loop given in Fig. 11. In that case, the current step response would be critical-aperiodic and without overshoot.

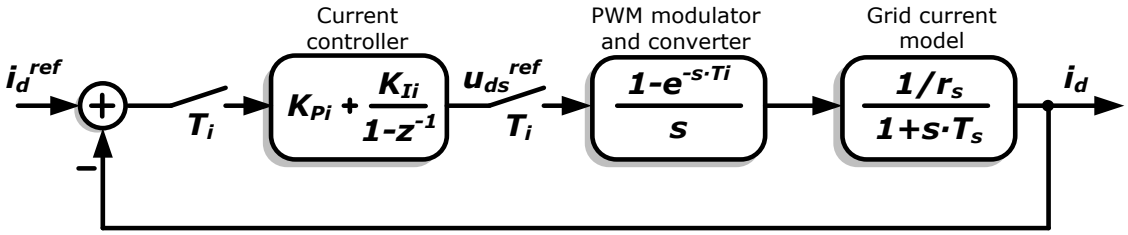

Fig. 11. Block diagram of current control loop.

The PI controller parameters are calculated according to expressions (10)-(12):

$$PI_{id}(z) = PI_{iq}(z) = K_p\left(1 + \frac{K_i}{1 - z^{-1}}\right) \quad (10)$$

$$K_{Pi} = \frac{\left(1 - e^{-\lambda T_i}\right)}{K\left(e^{T_i/T_S} - 1\right)} \quad (11)$$

$$K_{Ii} = e^{T_i/T_S} - 1 \quad (12)$$

where K is the total gain in an open-loop system ($1/r_S$), and λ is a parameter which determines the response time of a current closed-loop (where ($1/\lambda$) is the desired time constant of a current closed-loop). Usually, $1/\lambda$ takes the value of $T_{DC}/5$, where T_{DC} is the sampling period of the outer, dc-link voltage loop, in order to have a stabilized and settled current value in one dc-link voltage sampling period. This enables independent design of current and dc-link voltage control loops.

Experimental Results

In order to evaluate the behavior of the current-control loop, the system given in Fig. 12 was created using the Schematic Editor. A constant dc-link voltage source is placed in front of the grid-connected inverter. In this test phase, we want to evaluate only the system's current loop, independently, without regard to the dc-link voltage control loop. The RL passive elements shown here include the coupling and grid resistance and inductance values. Their values (*Ra = Rb = Rc = 0.01 Ω, La = Lb = Lc = 20 mH* in this example) determine the controlled-object transfer function in the current control loop, as depicted previously in Fig. 11.

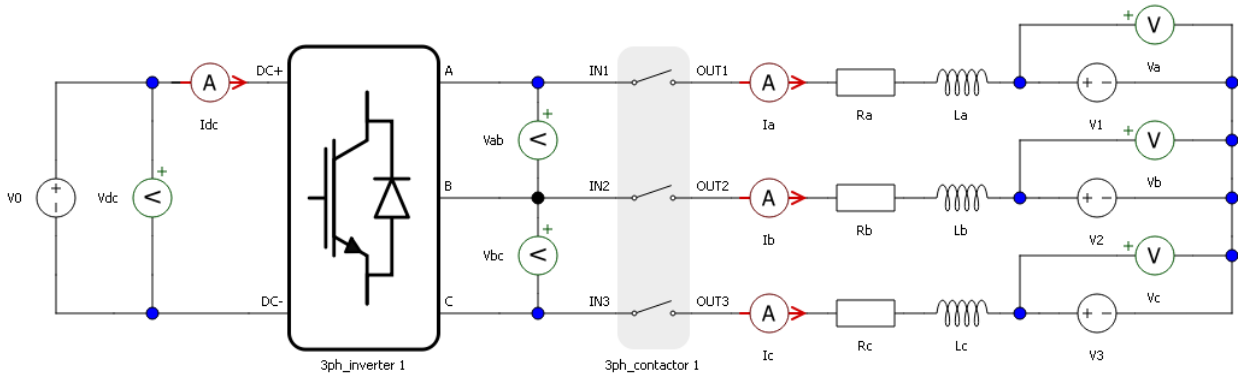

Fig. 12. Controlled system overview: schematic used for current-control-loop test.

Fig. 13 gives the current step response for PI controller parameters adjusted according to Dahlin's algorithm. Step reference of 0.4 p.u. is commanded to current *d*-component (i_d), while quadrature current (i_q) reference is set to zero (controller current base value is I_B = *7.5 A*).

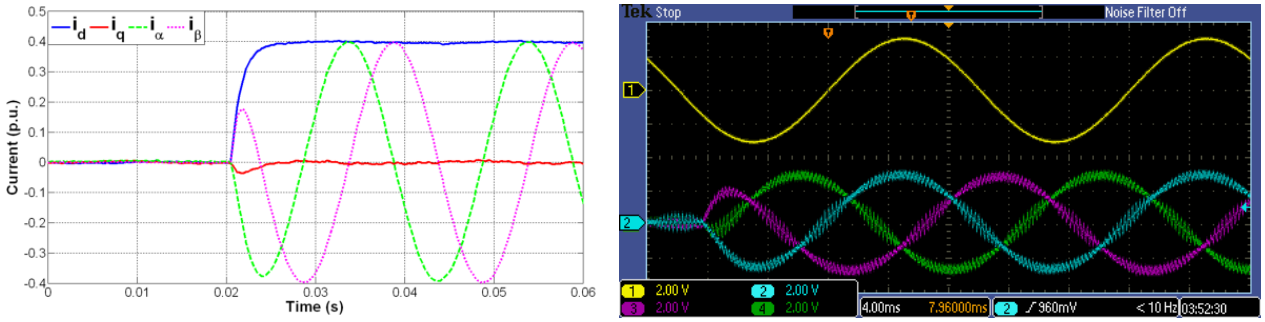

(a) (b)

Fig. 13. Current control loop test: system variables in the case of PI controller parameters adjusted according Dahlin's algorithm (Kp = 0.1769, Ki = 1.25e-4). The applied current step for d-axis current i_d (a) produces the response in grid phase voltage and currents shown on the oscilloscope (b).

In part a of Fig. 13, it should be noted that the *d*-axis current (i_d) response is critical-aperiodic with a settling time of 5 ms, which is consistent with the selected design parameters ($\frac{1}{\lambda} = T_{dominant} = T_{DC}/5, T_{DC} = 5ms$). The current *q*-component (i_q) has a stable zero value as commanded, after a short transient period. This indicates that decoupled and independent control of dq-current components was achieved successfully. The amplitude of currents in the $\alpha\beta$ stationary reference frame has the same value as the current amplitude in the *d*-axis, since there is an applied *abc/dq*-transformation invariant to amplitude.

Part b of Fig. 13 shows relevant HIL model signals captured with the oscilloscope (in parallel with recording controller variables in part a of the figure): Ch1 = V_a, Ch2 = i_a, Ch3 = i_b, and Ch4 = i_c. HIL scaling coefficients are set to *100 V/*V_{HIL} for voltage and *1 A/*V_{HIL} for currents. It can be verified that the current amplitudes really equal the reference values (i_{dref} =0.4I_B = 3 A; scope: i_{abc} ≈ 1.5 div x (2 V/div) x (1 A/V_{HIL}) = 3 A.) One must note that, in this case, phase-a current (*Ia*) is in phase with phase-a voltage (*Va*), which indicates that the *d*-current component determines active power flow between the converter and the grid.

Current ripple noise on the PWM frequency (4 kHz) also can be evaluated, and this information can then be used for selection/design of appropriate coupling elements (inductance). This could be one example of using HIL emulation for testing some hardware-based functionalities of the grid-connected converter.

Fig. 14 shows the inverter injected output phase-to-phase (*Ch1 = Vab*) and phase (*Ch2 = Va*) voltage, and injected phase current (*Ch3 = Ia*) for the case where reference current *d*-component is set to 0.4 p.u. (*3 A*). It should be noted that HIL emulates the inverter switching model, by sampling the controller's PWM signals even

below the emulation time-rate of *1 µs* in order to provide a more realistic model (T_{s_pwm} = *100 ns*). This high emulation rate can be noted in the zoomed-in section of Fig. 14, especially in the current signal where there are noticeable micro-steps (at a *1-µs* rate) in the current ripple value.

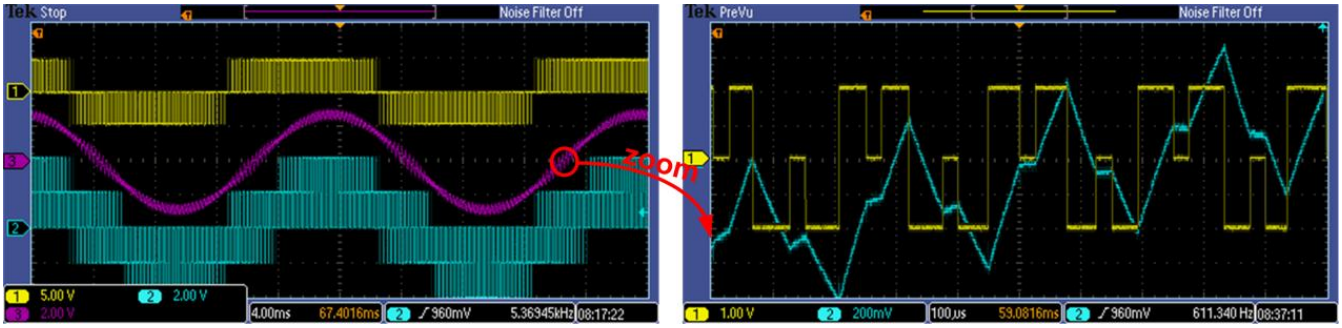

Fig. 14. Inverter PWM modulation test (PWM period = 250 µs, HIL emulation time-step = 1 µs, HIL digital inputs (PWM signals) sampling time = 100 ns).

In Fig. 15, the current step response for a case with unadjusted PI controller parameters is shown. It can be concluded that, due to the higher PI parameter values, current in *d*-axis has significant overshoot, which can lead to undesirable power oscillations between the converter and the grid in this type of application.

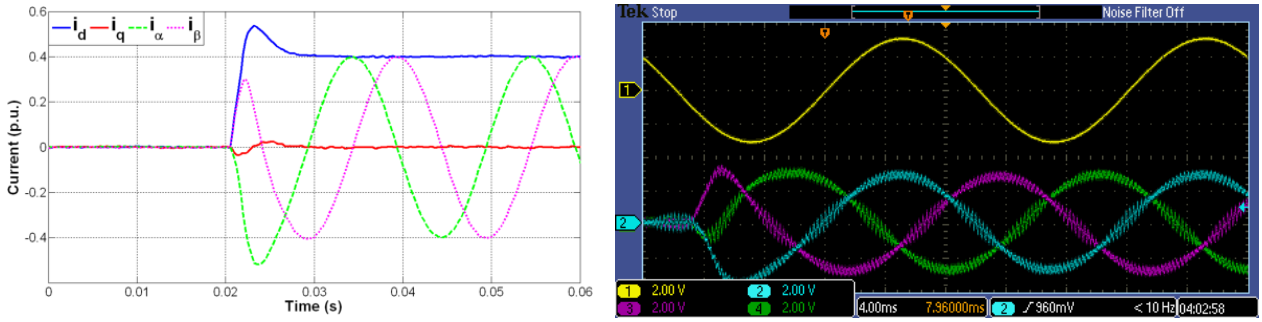

(a) (b)

Fig. 15. Current control loop test: system variables in the case of unadjusted PI controller parameters (Kp = 0.3, Ki = 0.1). The applied current step for d-axis current i_d (a) produces the response in grid phase voltage and currents shown on the oscilloscope (b).

DC-Link Voltage Control Loop Test

Technical Background

In order to have a linearized control loop, instead of regulating the dc-link voltage, the energy flow through the dc-link is regulated. As an absolute value, the dc-link energy is expressed as:

$$e_{DC} = \frac{1}{2} C_{DC} u_{DC}^2 . \qquad (13)$$

Since the derived base value for the energy variable is:

$$E_B = P_B T_B, \quad T_B = \frac{1}{\omega_B} \qquad (14)$$

the normalized expression for the dc-link energy has the same form as in the absolute domain (where P_B is the power base value and ω_B is the angular frequency base value.) If converter losses can be neglected, the dc-link capacitor energy can be expressed as in (15).

$$e_{DC} = \int p_{DC} dt = \int p_G dt \text{ where } p_G = u_{dG} i_d \quad (15)$$

Since the grid voltage is constant or has small changes, the energy reference will actually produce an i_d current reference. Therefore, the dc-link voltage control loop has a layout as depicted in Fig. 16. It is very similar to the speed control loop of ac drives. Here, energy is the integral of the power, i.e. i_d current, and in vector-controlled drives, speed is the integral of the electromagnetic torque, i.e. i_q current.

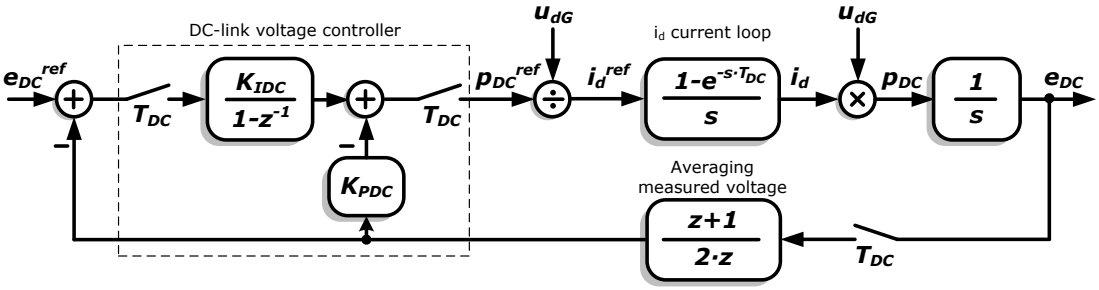

Fig. 16. DC-link voltage (energy) control loop.

The reference energy value depends on desired dc-link voltage value as in equation 16:

$$e_{DC}^{ref} = \frac{1}{2} C_{DC} (u_{DC}^{ref})^2 \quad (16)$$

The scheme from Fig. 16 can be transformed into the discrete domain as depicted in Fig. 17.

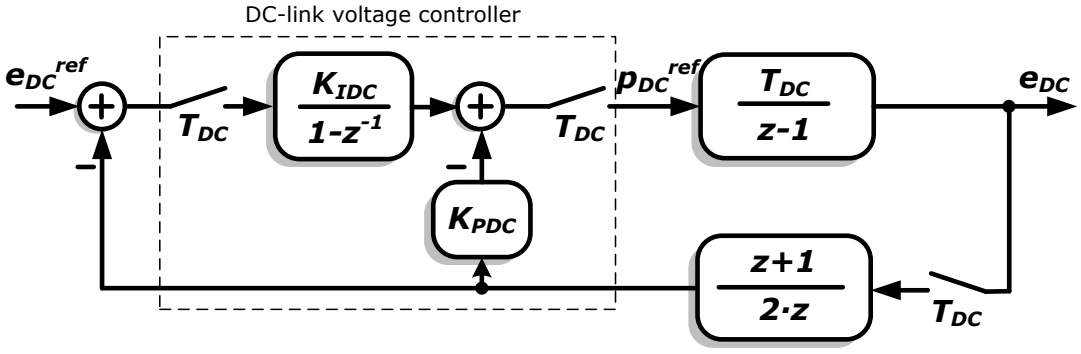

Fig. 17. DC-link voltage (energy) control loop in discrete domain.

Controller parameters are determined using the optimization procedure that results in an aperiodic response with the maximum possible speed. In fact, all three poles of the system characteristic equation are set to be real and equal. Consequently, proportional and integral gains of the dc-link voltage controller are given in (17) and (18):

$$K_{pDC} = \frac{K_1}{K^*} \quad (17)$$

$$K_{IDC} = \frac{K_2}{K^*} \quad (18)$$

where K_1 = 0.203, K_2 = 0.035 and $K^* = T_{DC}/2$.

Experimental Results

Fig. 18 shows the step response of a dc-link voltage control loop for a change in reference value. The test circuit emulated in the HIL is the same as in Fig. 3, with capacitor *C = 1000 μF* in the converter dc-link. The dc-link voltage step reference is commanded from *0.866 p.u.* (the default initial value of capacitor voltage is set to *650 V*, and the controller base voltage is set to U_B = *750 V*) to 0.95 p.u. (*712.5 V*), while the reactive power reference is set to zero.

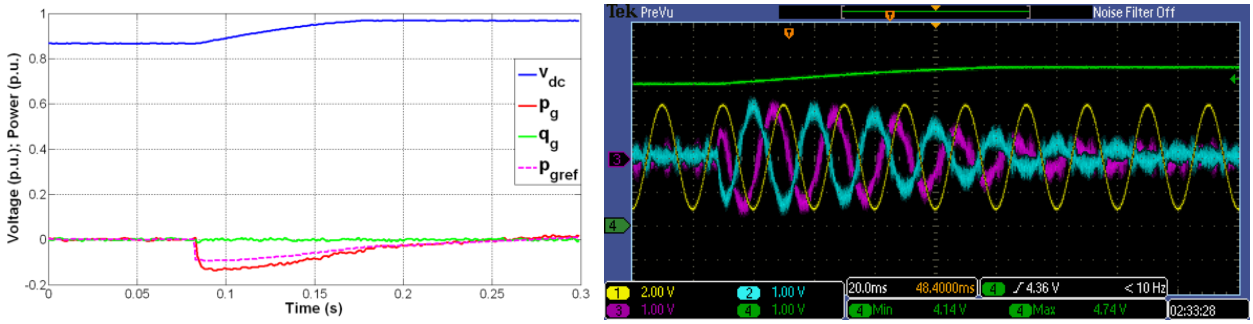

(a) (b)

Fig. 18. DC-link voltage control loop test: reference step response.

In part a of Fig. 18, it should be noted that the dc-link voltage reference is achieved with no overshoot. In order to charge the dc link capacitor to a new reference value higher than the initial value, there must be active power flow from the grid to the converter (i.e. it has negative value during transition process), while reactive power is zero as commanded.

In part b of Fig. 18, the relevant HIL model variables for testing the dc-link control loop are observed on the scope: *Ch1* = V_a, *Ch2* = i_a, *Ch3* = i_b, *Ch4* = V_{DC}. The HIL scaling coefficients used here are *100 V/*V_{HIL} for voltage V_a, *150 V/*V_{HIL} for voltage V_{DC} and *1 A/*V_{HIL} for inverter, i.e. grid currents. It can be concluded that phase currents are equal to zero before and at the end of the transition process, indicating a stable dc-link voltage value. During the transition process one can note that grid currents have inverse phase compared to the corresponding grid phase voltages, indicating active power flow in the direction from the grid to the converter dc-link.

In order to evaluate the disturbance rejection of the dc-link voltage control loop, the system given in Fig. 19 is created in the Schematic Editor and downloaded/emulated on the HIL. The constant dc-link voltage source is now replaced by the capacitor and current source whose value is varied to model the desired disturbance. Typhoon HIL actually enables the user to evaluate a complete PV inverter system, by replacing the current source with a PV panel model (with, for example, a boost dc-dc converter stage), or a complete energy storage system, by replacing the current source with a battery model.

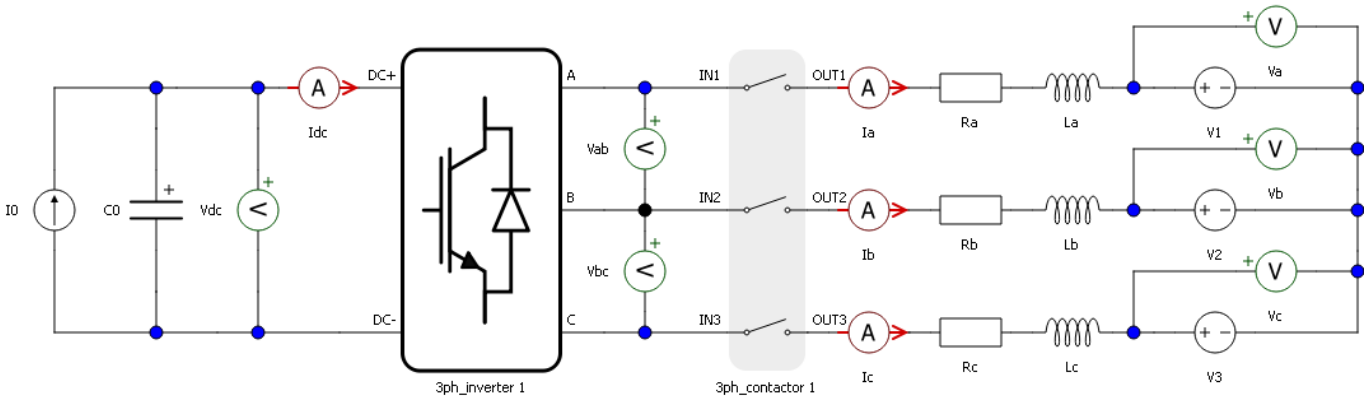

Fig. 19. Disturbance rejection test for dc-link voltage-control loop: a system overview.

Fig. 20 shows two cases for dc-link voltage-control-loop disturbance test recorded by the scope on the HIL analog outputs. In part a of the figure, signals are given for the situation where the dc current source reference (I_0) is set from zero to 2 A, while part b of the figure shows the situation where the current source reference is set from 2 A to zero (*Ch1* = V_a, *Ch2* = i_a, *Ch3* = i_b, *Ch4* = V_{DC}.) The HIL scaling coefficients used are *100* V/V_{HIL} for voltage V_a, *150* V/V_{HIL} for voltage V_{DC} and *1* A/V_{HIL} for the currents.

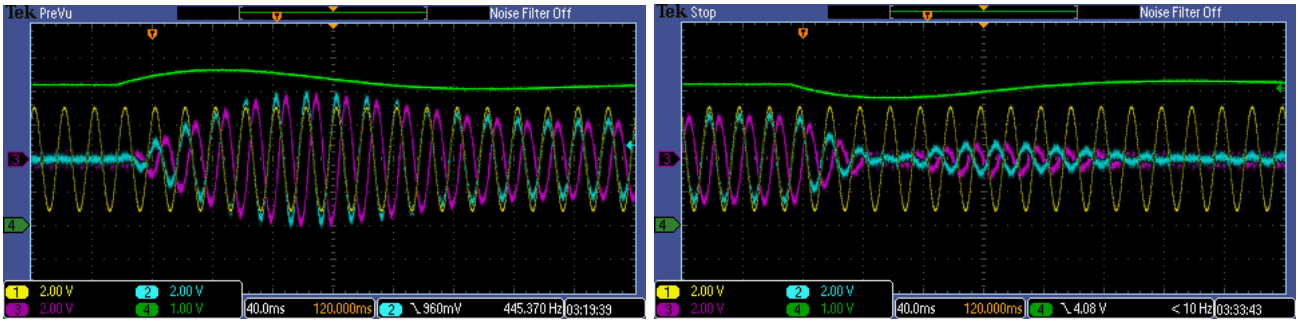

Fig. 20. DC-link voltage-loop-disturbance rejection test. Results are shown for a dc current source stepup from 0 A to 2 A (a) and for a stepdown from 2 A to 0 A (b).

The dc-link voltage was maintained to its default, nominal value of 650 V. It can easily be concluded that the dc-link voltage-control loop manages to keep this voltage constant. Grid currents are zero when the dc current has zero value, while they are in-phase (or with inverse phase) with corresponding phase voltages when the dc current has a non-zero value, indicating active power flow between the grid and the converter. During the dc-link voltage steady-state, all incoming energy from/to the current source is supplied to/from the grid, which represents the main task in grid-connected converter applications.

Summary

This article showed some of the ways in which the Typhoon's ultra-high-fidelity real-time HIL emulation hardware (with 1-µs time-step) and related software tool-chain offers advanced development and testing capabilities to manufacturers of grid-connected converter systems. By using the presented test environment, developers now can produce adequately tested grid-connected inverters that can satisfy variable and more stringent regulatory and operational requirements. And all of that can be accomplished in an automated way (using Typhoon's scripting tool) and under extremely reduced R&D and QA cost and time.

About The Authors

Evgenije M. Adžić received the Dipl.-Ing and M. S. degrees in electrical engineering from the Faculty of Technical Sciences, University of Novi Sad, Novi Sad, Serbia in 2005 and 2007, respectively. In 2005, Evgenije joined the Faculty of Technical Sciences, University of Novi Sad, Serbia and since September 2007, he has been a Ph.D. student at the Chair for Power Electronics and Electrical Machines at University of Novi Sad. In 2010, Evgenije joined Typhoon HIL in Novi Sad where he currently serves as director for Power Electronics Application Engineering and Quality Assurance Group. His interests are in the field of power electronics, renewable energy sources, and ultra-low-latency hardware-in-the-loop systems.

Vlado B. Porobić received the B.S., M.S and Ph.D. degrees in electrical engineering from the Faculty of Technical Sciences, University of Novi Sad, Serbia, in 2000, 2005, and 2011, respectively. From 2000 to 2011, Vlado was employed on the Faculty of Technical Sciences, as a teaching and research assistant in the Department for Power Electronics and Electrical Machines. Since 2011 he has been with Typhoon HIL in Novi Sad where he is working as a power electronics application engineer, developing various control applications for testing and evaluating HIL models and accompanying software. His main research is focused in the area of power electronics and motor control.

Nikola L. Čelanović received a B.S. degree in electrical engineering from the University of Novi Sad in 1995, an M.S. degree in Mechanical Engineering from Vanderbilt University, Nashville, Tennessee in 1996 and a Ph.D. degree from Virginia Polytechnic Institute and State University in 2000. From 2000 to 2005 Nikola was with the ABB Research Centre in Baden-Dättwil, Switzerland and from 2005 to 2008 with the ABB Drives Development Department, Turgi, Switzerland. Since 2008 Nikola has been the CEO and co-founder of Typhoon HIL in Baden, Switzerland.